RSC Advances

ROYAL SOCIETY OF CHEMISTRY

www.rsc.org/advances

Optimizing the prepared condition of TiO_2 1D/3D network structure films to enhance the efficiency of dye-sensitized solar cells

Baoyuan Wang, Jingshu Wan, Jun Zhang, Hao Wang*

Hubei Collaborative Innovation Center for Advanced Organic Chemical Materials, Faculty of Physics and Electronic Science, Hubei key laboratory of ferroelectric and dielectric materials and devices, Hubei University, Wuhan 430062, PR China

*corresponding author: Hao Wang; Telephone: +86027-88662550; Fax number : +86027-88663390; Email: nanoguy@126.com;

Abstract:

A novel structure of TiO_2 films have been successfully prepared on a fluorine-doped tin oxide (FTO) glass substrate through a feasible two-step hydrothermal method. The first-step hydrothermal growth results in rutile TiO_2 one-dimensional (1D) rutile TiO_2 nanorod arrays capped by 3 dimensional (3D) rutile TiO_2 nanorods, and the second-step hydrothermal etching in hydrochloric acid solution leads a selective etching of 3D TiO_2 nanorods to form 3D nanotubes at first, and then the tip wall of the nanotubes divide into secondary nanowires with reduced diameter. The resultant bi-layer TiO_2 network structure films were served as photoanodes in dye-sensitized solar cells (DSSCs). The 3D rutile network structure provides large surface area for dye-loading and the oriented nanorod arrays at the bottom layer enables direct pathway for electron transport. The influence of etching time toward the photovoltaic performance of the DSSCs fabricated from TiO_2 network structure films has been comprehensively studied. It was found that the mount and the length of secondary nanowires reached a maximum when the etching time was 14 h, which resulted in the largest surface area and best dye-loading ability of the TiO_2 network structure films,

producing overwhelming power conversion efficiency (PCE) of 5.71%. In addition, the $TiCl_4$ post –treatment was employed to further improve the PCE. Through optimizing the amount of the titanium precursor and the time of $TiCl_4$ treatment, the DSSCs assembled by TiO_2 1D/3D network structure photoanode presented a markedly enhanced efficiency of 7.68%, when the TiO_2 films was synthesized at 0.9 ml tetrabutyl titanate following by 12h etching and treated with $TiCl_4$ for 48h.

Keywords: TiO_2 1D/3D network structure; etching treatment; dye-sensitized solar cells; surface area;

1. Introduction

DSSCs have attracted much research attention and are considered as a prospective alternative to silicon-based solar cells due to its dominant superiority including free-pollution, low-cost, and relatively high-efficiency [1-5]. The conventional photoanodes of DSSCs are made from TiO_2 nanoparticles films, which suffer from severe photo-generated electron recombination because the interfaces between nanoparticles can serve as traping-detraping site for electrons [6, 7]. In order to overcome this problem, 1D TiO_2 nanorod arrays with a rutile phase are widely utilized as the photoanode in previous work [8-12], which can provides a direct electrical pathway and facilitates electron transport. However, TiO_2 nanorod arrays photoanode is subjected to a vital shortcoming, i.e. low surface area, comparing with TiO_2 nanoparticle photoanode as the similar thickness. Thus, the photovoltaic performance of DSSCs fabricated from single–crystalline rutile TiO_2 nanorod arrays is still lower than those of nanoparticle-based photoanode. A number of groups have reported methods to improve the surface area of 1-D rutile TiO_2 nanorod arrays [13, 14]. For example, Hong et al used a single step hydrothermal route to synthesize 3D nanostar/1D nanorod

network structure and found that the addition of 3D nanostars on 1D nanorod arrays significantly improved the surface area, demonstrated an excellent PCE of 5.39 %, which is markedly greater than the cells constructed from a pure 1D nanorods photoanode (3.74 %) [15]. Sun research group reported a bi-layer photoanode involving 1D nanowires and 3D dendritic nanostructures, which yielded a enhanced PCE up to 7.2 % [16]. In this way, the incorporation of 3D network structure layer such as 3D nanostars and 3D dendrites on the 1D nanorod arrays is regarded as an effective strategy for improving the surface area of TiO_2 films. In addition, chemical etching treatments is also usually used for enlarging the surface area of rutile TiO_2 nanorods. For example, Lin et al developed an etching treatment in hydrochloric acid for TiO_2 nanorod arrays, which induced the nanorods with big diameter splitting into lots of small nanorods, consequently resulted in the remarkable enhancement of specific surface area of TiO_2 nanorod arrays, and in turn allows the increase of dye-loading ability of TiO_2 nanorod photoanode [17, 18].

In this work, we directly synthesized TiO_2 1D/3D nanorods on the FTO substrate using a typical hydrothermal way, and second-step hydrothermal etching was employed for the sake of large specific surface area. The resultant bi-layer configuration possessed a bottom layer of 1D nanowire arrays providing a direct electrical pathway and flower-like 3D nanostructure on top layer exhibiting a large surface area for dye-loading. By applying the TiO_2 1D/3D network structure films with superior electron-transport rate and excellent dye-loading ability in the DSSCs, a markedly high PCE of 7.68% was obtained after optimizing the amount of titanium precursor and the time of $TiCl_4$ post-treatment.

2. Materials and Methods

2.1 The preparation of TiO_2 1D/3D nanorods on FTO glass substrate

The hydrothermal method, presented by Guo group, was used to synthesize 1D/3D nanorods on FTO glass substrate [19]. In a typical process, 16 ml deionized (DI) water and 16 ml hydrochloric acid with 36.5 wt%-38wt% concentration was added to a beaker, and then stirred for 5 min to form homogenous mixture. Amount of tetrabutyl titanate was dropped into this solution as a titanium precursor. After stirring for another 5 min, the mixed solution was enclosed in a Teflon-lined autoclave (50 ml capacity) in which a piece of FTO glass substrate (2×2 cm^2) was flatly placed with conductive side faced up. The reactor was transferred into an electrical oven, and maintained the temperature at 150 ^oC for 10 h. Waiting for the reactor cooling down, we take out the FTO glass substrate grown by TiO_2 films, and immersed the resultant films in DI water for 2 h to remove the residual acid. Finally, the TiO_2 films were subjected to a 2 h annealing treatment at 500 ^oC under air atmosphere, and designated as 1D/3D nanorods sample.

2.2 Hydrothermal etching treatment

To increase the surface area, an acid etching treatment was conducted to the as-prepared samples [20]. Briefly described, 5 ml DI water was mixed with 11 ml hydrochloric acid with concentration of 36.0-38.0 wt %, following a 5 min stir to form a homogenous etching solution. The as-prepared TiO_2 1D/3D nanorods were immersed into this solution and suffered from a hydrothermal etching treatment at 150 ^oC for 8-16 h. After the etching reaction finishing, the sample was take out and immersed in DI water for 2 h.

2.3 Transferring the TiO_2 films to a new FTO glass substrate

The hydrothermal etching treatment results in TiO_2 paper-like films detached from the FTO

glass substrate. These free-standing TiO_2 films with a network structure were carefully transferred to a new FTO glass, which was pre-covered by an ultra-thin layer of TiO_2 paste with good viscosity [21, 22]. Finally, the TiO_2 films were annealed at 500 ^oC in air for 2 h..

2.4 Dye sensitized solar cell fabrication

The previously described photoanode of the TiO_2 films on FTO substrate was immersed into 0.3 mM ethanol solution of Ruthenium dye (N719) and maintained for 24 h at room temperature. Then, the samples were taken out and rinsed with ethanol to remove the un-adsorbed dye molecules. Platinum films sputtered on FTO substrate was served as a counter electrode and face to face bonded with the N719-sentizied TiO_2 photoelectrode. Finally, the iodide-base electrolyte was injected into the free space between the two electrodes to complete the cell fabrication. The active area of the solar cell was approximately 0.16 cm^2.

2.5 Characterization

The crystalline structure of the TiO_2 samples was characterized using an X-ray diffractometer (XRD, Bruker D8). The morphological observation was conducted by a field-emission scanning electron microscope (FESEM, JSM-7100F, JEOL). The diffused reflectance spectra and the amount of dye-loading on TiO_2 photoanode were examined by UV-vis spectrophotometer (UV-3600, Shimadzu). Brynauer-Emmett-Teller (BET) surface areas were determined by an ASAP 2010 nitrogen adsorption-desorption apparatus. The current density-voltage (J-V) characteristics of the DSSCs were recorded by a source meter (Keithley 2420) under the AM 1.5 solar simulator (Newport, 100 mW/cm) illumination. The incident-photon-to-current efficiency (IPCE) was tested by standard Measurement kit from Oriel Company. Electrochemical workshop (CHI-660D) was used for open-circuit voltage decay (OCVD)

measurements.

3. Results and discussion

3.1 The optimization of etching time

Figure 1s shows the SEM images of as-prepared TiO_2 1D/3D nanorods, which was synthesized at 150 ^oC for 10 h using a solution of 1.0 ml tetrabutyl titanate, 16 ml DI water and 16 ml concentrated hydrochloric acid. As the figure 1s shown, a bi-layer configuration was distributed uniformly on the FTO substrate after the first step hydrothermal synthesis. The upper layer of the structure was comprised of abundant 3D TiO_2 nanorods which looked like a natural chrysanthemum and the bottom layer contained densely high-aligned 1D nanorod arrays with a thickness of ~5.3 μm. For the purpose of large specific surface area, the as-prepared TiO_2 1D/3D nanorods were subjected to hydrothermal etching in a mixed solution of DI water and hydrochloric acid. The specific surface area and pore volume of TiO_2 nanostructure before and after etching treatment were measured by Brunauer-Emmett-Teller (BET) and Barrett-Joyner-Halenda (BJH) analysis using a nitrogen adsorption-desorption apparatus. The measured specific surface areas of the as-prepared TiO_2 1D/3D nanorods were 75.53 m^2g^{-1}. Through 12 h etching, the surface areas were improved to 134.06 m^2g^{-1}. The result indicates that the etching treatment was an effective method for larger surface area. In addition, time dependent experiments were conducted to study the relationship between the etching duration and the microscopy of the TiO_2 network structure, the temperature was maintained at 150 ^oC, while the etching time was varied from 8 to 16 h, and four samples had been prepared corresponding to 8 h, 10 h, 12 h, 14 h and 16 h, respectively. Figure 1 shows the plan-view of the TiO_2 network

structure etched for different times. As the figure 1a shown, several caves were observed on the top facet of TiO_2 nanorods after 8h etching. However, the profile of nanorods displayed no morphological change and remained smooth. Because the dissolved rate of (001) crystal facets in the rutile TiO_2 was much greater than that of (110) planes. In other word, the rutile TiO_2 nanorods would dissolved in HCl solution along the [001] direction but no [110] direction [23-25]. The walls between adjacent caves gradually dissolved in the hydrochloric acid as the etching process continued and the diameter of caves increased with etching time. Ultimately, several small caves connected each other to form a bigger one when the etching time reached 10h. It can be seen from figure 1b that the center part of nanorods had been hollowed out and the petal of 3D clusters had been transformed from nanorod to nanotube structure which displayed an diameter of ~300 nm and wall thickness of ~20 nm, the inner surface of nanotube can provide much more sites for dye-loading. It is worth noting that the tip wall of the tubes had split into secondary TiO_2 nanowires with smaller diameter at the meantime. As the hydrothermal etching time prolonged to 12 h, the amount and length of secondary nanowires began to increase, and they both reached a maximum value in the case of 14h. From the top view of figure 1d, it can be observed that the structure of nanotubes had been severely damaged and all of the samples were composed by lots of nanowires; there were significantly large surface area for dye adsorbing across the entire 3D nanowires film. However, when the etching duration was further extended to over 16h, the secondary nanowires were rapidly dissolved in HCl solution under the hydrothermal condition and the 3D TiO_2 in upper layer returned to the nanotube structure. Obviously, the depth of this nanotube was greater than that of 10h etching sample, but the total length of the nano-petal decreased and some cracks emerged at the root of nanotube, due to the

long time corrosion in the hydrochloric acid solution. By observing the morphology of samples with different etching durations, the etching process of the nanorods can be understood as follows. At early stage, the center portion of the nanorods was cut off by hydrochloric acid and the nanorods had been transformed into nanotubes structure, the depth of nanotube increased with the etching duration. When the etching time was prolonged, the upper part of the nanotube wall would split into secondary nanowires with small diameters, which led to more and longer nanowires. In the meantime, the tip of secondary nanowires would dissolve in the hydrochloric acid during the hydrothermal process. At the initial etching process, the rate of splitting was higher than the speed of nanowires dissolution, so the amount and length of the nanowires increased with etching time in the early phase. As the etching continued, the splitting speed gradually decreased, and balanced with the dissolution rate, then the system approached equilibrium. At this point, the most and longest nanowires were obtained. Further prolonging the etching time, the nanowire dissolution rate continually increase and higher than the production rate, causing the secondary nanowires gradually disappeared.

Figure 2 presents the cross-sectional views of the TiO_2 nanorod arrays on the bottom layer after the etching treatment in hydrochloric acid solution at 150 ^oC for various times. For the 8 h etching sample, the length of the nanorods was 5.2 μm, which exhibited little change compared with the virgin sample. However, it is worth noting that the original TiO_2 nanorod had split into lots of nanorods with reduced diameters. Obviously, the hydrothermal etching lead to the compact nanorod arrays became loose, and the interstitial space between the adjacent nanorods dramatically amplified especially for the upper half part of TiO_2 nanorod arrays, resulting in large surface area for the TiO_2 nanorod arrays. When the hydrothermal etching duration was extended to

10, 12, 14 and 16 h, the thickness of the nanorod arrays was around 4, 3.3, 2.6 and 1.5 μm, respectively. It demonstrated that the length of the nanorod arrays decreased with the post-etching time afterward. In addition, when the etching time was prolonged to 16h, the bottom layer lost the structure of nanorod array and the bottom layer looked like dendritic.

The microstructure of the un-etched and 8 h etched TiO_2 network structure films were characterized by XRD instrument as shown in figure 3. For the as-prepared TiO_2 1D/3D nanorods samples, the XRD pattern can be assigned to the standard tetragonal rutile phase (JCPDS No.89-4920). Moreover, the 8h etched samples exhibited almost the same diffraction peaks locations as that of un-etched sample regardless of the difference in intensity; it can also be indexed to pure rutile phase. The result indicated that the post-etching had not destroyed the crystalline structure of TiO_2 films. Even if the etching duration was prolonged to 16 h, the TiO_2 films still remained the rutile phase as the figure 2s presented. As previous reports, the TiO_2 with rutile phase had unique advantage in the photoanode utilization, including better performance in light scatter and excellent chemical stability comparing with the anatase TiO_2 [26, 27]. The figure 2s revealed the XRD patterns of TiO_2 films etched for different times. As the figure 2s shown, Besides the diffraction peaks indexed to rutile TiO_2 labeled by Etta, the diffraction peaks of FTO substrate marked by Pound can also be found for the 8 h etched sample. It is well known that the intensity of diffraction peaks strongly depended on the amount of the sample. In the un-etched sample, the large quantity of TiO_2 leads to a high intensity of TiO_2 rutile diffraction peaks, which can shadow the peaks of the FTO substrate. During the etching process, a portion of the TiO_2 nanorods dissolved in the hydrochloric acid solution under hydrothermal condition as the SEM shown. The decrease in TiO_2 amount will significantly enhance the relative intensity of the FTO

peaks. This analysis can be validated by the XRD curves of the TiO_2 films etched for different times. It can be seen from figure 2s that the intensity of TiO_2 peaks decreased as the etching-time increasing and the FTO diffraction peaks displayed a reverse trend with etching duration.

The light-scattering capacity of photoanode has significant influence on the light-harvesting behavior of photoelectrode after dye sensitizing, which can be characterized by diffused reflectance spectra of the photoanode [28-31]. When the incident light irradiates on the photoelectrode (photoanode sensitized by dye), the photoanode with superior light-reflectance capacity should exhibit a high probability for capturing the incident light, which can lead to the enhancement of short circuit current density (J_{sc}) [32]. Figure 4 (a) displays the diffused reflectance spectra of TiO_2 network structure film etched for various times before dye adsorption. It can be observed that all the samples present an excellent reflectance ability with values larger than 70% in the visible light region, it should attributed to the relatively random packing of TiO_2 3D nanostructure in the top layer, which acts as an effective light-scattering layer. Amplifying the curves in 600-900 nm wavelength regions as the inset image shown, it can be found that the diffused reflectance slightly decreased with the etching time, possibly due to the decreased length of the TiO_2 nanostructure, including the nano-petal of the 3D nanostructure in top layer and the nanowire arrays in bottom layer. In addition, we can note that the reflectance of the 16 h etched sample was significantly reduced compared to the other four samples. The absorption spectra of the dye-sensitized TiO_2 films etched for different times are shown in figure 4 (b). It can be seen that the 14h etched sample presents the highest light absorbance in the wavelength range of 300-800 nm, which is mainly due to its excellent light-scatter ability as diffused reflectance curve shows and the superior dye-loading ability, which is validated in the dye-loading analysis as

shown in table 1. The peaks located at 380 nm and 530 nm are the characteristic absorption of the N719 dye.

Figure 5a presented the current density-voltage curves of DSSCs fabricated from TiO_2 network structure films with various etching time under the illumination of AM 1.5 solar simulator (100 $mWcm^{-2}$), the detail parameters were calculated from J-V curves and summarized in table1. The worthy noting point was that the etching time had no significant effect on the open circuit voltage (V_{oc}) values of these DSSCs, the four samples etching for 8, 10, 12 and 14 h displayed identical V_{oc} of about 0.73 V and the V_{oc} of the 16 h etched sample slightly reduced to 0.71 V. In addition, we can found that the J_{sc} presented an obvious difference among all the samples. The J_{sc} of DSSCs based on 8, 10, 12, 14 and 16h photoanodes was 8.37, 10.38, 11.95, 12.78 and 9.92 mA/cm^2, respectively, which gave rise to the corresponding PCE of 4.30, 5.25, 5.68, 5.71 and 4.51%. It can be found that the J_{sc} increased initially with the etching time from 8h to 14h and then decreased as the etching duration was further extended to 16 h. The commonly accepted viewpoint is that the J_{sc} value is mainly dependent on the light absorption of photoelectrode, which is strongly related to the amounts of dye molecules attached on photoanode, i.e. dye-loading ability. The superior dye adsorption is expected to generate more photo-generated carrier which result in the enhancement of J_{sc}. The dye-loading is determined from the absorbance curves of the dye desorption solution and calculated using the Lambert-Beer Law [33, 34]:

$$A=KCL \qquad (1)$$

Where K is the molar extinction coefficient of N719 at 515 nm, equaled to 1.41×10^4 $dm^3mol^{-1}cm^{-1}$, A is the absorbance of the N719 dye desorption solution at 515 nm, L is the length of cuvette used for absorbance spectra measurement. The calculated results were listed in last column of table 1.

As the etching time increasing from 8 to 14 h, the amounts of absorbed dye increased from 125.13 to 214.62 nmol/cm^2, and then decreased to 162.86 nmol/cm^2 when etching duration further extended to 16 h, the 14 h etched TiO_2 network structure exhibited the highest dye-loading. As the analysis of figure 1, the growth rate of secondary nanowires was balanced with its dissolved rate when the etching time was 14 h. At this point, the amount and the length of secondary nanowires reached the maximum value, the highest surface area was achieved and the most dye was adsorbed on the surface of TiO_2 films. Moreover, a noteworthy point is that the amount of dye absorption exhibited the same varied trend with that of J_{sc} and PCE. As is well known, although there are many factors influenced the J_{sc} value, the J_{sc} is nearly proportional to the amount of dye-loading which is a key factor for achieving high performance DSSCs.

Figure 5b shows the IPCE results for the five DSSCs assembled from TiO_2 network structure films with various etching time in the wavelength range of 400 to 800 nm. All the IPCE curves display the identical spectral shapes and achieve a peak at approximately 530 nm, which consistent with the characteristic absorbance of the dye N719. The curves exhibit the order of 8 h>16 h>10 h>12 h>14 h within the visible light region, which well agree with the order of J_{sc}. In fact, J_{sc} can be described by integrating the product of the incident photo flux density $\Phi_{ph,AM\ 1.5G}$ and IPCE (λ) of the cell over the wavelength (λ) of the incident light [35], expressed as:

$$J_{sc} = \int IPCE(\lambda) e\phi_{ph,AM1.5G}(\lambda)\,\mathrm{d}\lambda \quad (2)$$

Where q is the electron charge, the value of IPCE has a fixed order in the wavelength range of 400-800 nm as the IPCE curves shown, so it is easy to understand why the J_{sc} and IPCE exhibit the same order. It is worth mentioning that the 14 h etched sample exhibited the highest IPCE value among the five samples, which can be attributed to its greatest amount of dye molecule

loading and highest light reflectance, all the reasons resulted in the largest J_{sc}.

From the process of converting light to electricity in solar cells, it is well known that he photo-generated electrons will accumulate in TiO_2 photoanode under open circuit condition, and the remaining holes in the dye will be oxidized by the redox couple of electrolyte with the catalytic function of Pt counter electrodes, so that the dye and counter electrode can mountain electrical neutrality. The potential difference between photoanode and counter electrode generates the OCV. When the incident light is instantaneously turned off, the OCV will gradually decay over time, since the accumulated electrons in photoanode will be recombined by the trapped state of the cells, so the decreasing rate of the OCV is directly related to the velocity of electron recombination, i.e. the lifetime of electron. The OCVD method has been considered as a powerful tool to research the electron recombination in DSSC and can offer some detail parameter about the electron lifetime. We conducted this measurement in accordance with the technology developed by Zaban et al [36, 37]. In the typical experiment of OCVD, the solar simulator illuminated the DSSCs until the OCV reached a steady value, and then the incident light was instantaneously cut off using a shutter and the transient decay of the consequent photovoltage was recorded by an electrochemical workstation per 20 ms interval. The response time can be calculated by the following expression (3):

$$\tau_n = \frac{-K_B}{e}\left[\frac{dV_{oc}}{dt}\right]^{-1} \quad (3)$$

Where K_B expresses the Boltzmann constant equaled to 1.38×10^{-23} J/K, T is the Kelvin temperature, K_BT gives the thermal energy, e is the electrical quantity of elementary positive charge, it taken to be 1.69×10^{-19} C and dV_{oc}/dt is the derivative of the OCV with respect to time. Figure 6b showed the electron lifetimes as function of photovoltage for the samples etched for

different times. It can be seen that the electron lifetime decreased with etching duration increasing in the voltage range of 0.2-0.45 V. As the SEM image (figure 2) shown, the amount of secondary nanowires at bottom layer decreased with etching time, and the one-dimension nanowire arrays can provide a direct pathway for electron transport. Thus, this decrease in secondary nanowires amounts can be regarded as the reduction of the pathways for electron transport, which should slow the electron transport velocity and increase the chance of electron recombination, ultimately leading to the decrease in electron lifetime. When the etching time was extended to 16 h, the nanorod arrays structure would have been severely damaged and the pathway for electron transport disappeared.

3.2 optimizing the amount of titanium precursor and the times of $TiCl_4$ post-treatment

To obtain superior DSSCs with excellent photovoltaic performance, the amount of titanium precursor added for 1D/3D nanorods synthesis was optimized. The etching-time was fixed at 12 h, while the amount of titanium precursor was set to 0.8, 0.9, 1.0 and 1.2 ml. The influence of titanium precursor amount toward the photovoltaic performance of the assembled DSSCs had been investigated. Figure 7 presented the typical J-V curves of these cells made from different titanium precursor amount and the details parameters of those cells were summarized in table 2. It can be found that the cells synthesized at 0.9 ml tetrabutyl titanate exhibited the highest J_{sc} of 13.47 mA/cm^2 and the largest V_{oc} of 0.76 V, which resulted in the highest recorded efficiency of 6.44%.

Many methods were developed to improve the photovoltaic properties of DSSCs; among all of these methods immersing the TiO_2 films in a titanium tetrachloride ($TiCl_4$) solution was regarded as the most effective way. After this modification, extra TiO_2 nanoparticles can be

synthesized through $TiCl_4$ hydrolysis on the surface of prepared TiO_2 films, which leads to further enlargement of the TiO_2 surface area. Consequently, it improves the amount of dye molecule adsorbed on photoanode surface. Moreover, several publications reported that $TiCl_4$ post-treatment can also improve the light scattering capacity and prevent the electrons in photoanode from recombining with electrolyte [38-40]. The above results indicated that the optimum preparation conditions of the TiO_2 photoanode was 0.9 ml of titanium precursor followed by 12 h etching treatment. In this work, $TiCl_4$ treatment was conducted to the TiO_2 network structure films prepared under the optimum conditions for further improvement in cell performance. We fabricated four samples by immersing the TiO_2 photoanodes in 0.1 M $TiCl_4$ solution at room temperature for 0, 12, 36 and 48 h, respectively. The resultant TiO_2 films were annealed at 450 ^oC for 30 min. Figure 8 displays the SEM images of the four samples modified with $TiCl_4$ for various times. It can be observed from figure 8a that the 3D nanorods had been transformed into nanotubes structure after etching treatment and the surface of nanotubes was smooth. After 12h $TiCl_4$ treatment, the profile of the nanotubes was attached with a lot of nanoparticles which roughened the surface and the size of the nanoparticles was about 10 nm. Moreover, the figure 8c reveals that the amount and the size of the nanoparticles increased with the immersion time. When the treatment duration prolonged to 48 h, the inside and outside surface of the nanotube was filled with a large number of TiO_2 nanoparticles. The more detailed morphology of the sample with 48 h $TiCl_4$ post-treatment is shown in figure 3s. It can be seen that the films maintained the 3D nanoflower structure, which was comprised of several nanotubes petals. Compared with the un-treatment sample, the inner diameter of this nanotubes decreased, which ascribed to the increased amount of TiO_2 nanoparticles attached on the inner surface of nanotubes. Figure 3s (a, b)

shows the top view and cross-sectional SEM images of the one-dimension nanowire arrays on the bottom layer after 48 h $TiCl_4$ treatment. It can be observed that the tip and the profile of the nanowire arrays were covered with abundant TiO_2 nanoparticles. In addition, the high magnification SEM images displayed that the average diameter of the TiO_2 nanoparticles was approximately 20 nm.

Figure 9 exhibits the J-V curves of the DSSCs assembled from TiO_2 photoanode which treated with $TiCl_4$ for different times and the corresponding photovoltaic parameters are listed in table 3. The noteworthy point here is that the $TiCl_4$ modification remarkably increased the J_{sc}, which reached a maximum value of 18.30 mA/cm^2 for the 48 h treatment sample. The J_{sc} increased with $TiCl_4$ post-treatment time can be explained as follow: as the SEM images (figure 8) shown, the $TiCl_4$ immersion gave rise to the hydrolysis of $TiCl_4$ and generating lots of TiO_2 nanoparticles attached on the TiO_2 films surface, involving the 1D nanowire arrays on the bottom layer and the 3D nanotubes on the top layer. Moreover, the amounts of TiO_2 nanoparticle increased with treatment time, which improved the specific surface of TiO_2 films, leading to the enhancement of dye-loading ability. In addition, it was found that the PCE values of DSSCs presented slight decrease when the $TiCl_4$ treatment time increased from 0 to 12 h, then increased as further prolonging treatment time to 36 or 48 h. Whereas the OCV and FF always exhibited a obviously decrease with $TiCl_4$ treatment times, it maybe due to the increase of the sheet resistance after $TiCl_4$ treatment. These results suggested that the increase of PCE was derived mostly from the enhancement of photocurrent density. Moreover, a thin TiO_2 layer was covered on the bare surface of the FTO substrate after $TiCl_4$ treatment, which blocked the recombination between electrons in photoanode and positive charge in electrolyte. In addition, modification using $TiCl_4$ can also

improve the light scattering capacity of the TiO_2 films. All these functions of $TiCl_4$ treatment resulted in high energy conversion.

4. Conclusions

TiO_2 films with 1D/3D nanorods network structure have been successfully prepared on transparent conductive FTO glass substrate via a facile one-step hydrothermal method. In order to further enlarge the surface area, an etching treatment was employed to the TiO_2 network structure films. Comprehensive studies concerning the effects of etching time on the performance of the TiO_2 network structure films were presented. The results showed that etching treatment using hydrochloric acid did not destroy the crystalline rutile properties of TiO_2 films. In addition, the light-scatter ability and electron-lifetime of TiO_2 films decreased as the etching duration increased. These were attributed to the reduced length of TiO_2 nanostructure, including the petals of 3D nanostructure in top layer and the nanowires in bottom layer. For the 14h etching sample, the splitting rate of secondary nanowires balanced with the TiO_2 dissolution velocity, the amount and the length of the secondary nanowires reached a maximum, which resulted in the largest surface area and best dye-loading ability of the TiO_2 network structure films. After optimizing the titanium precursor amount and the $TiCl_4$ post-treatment time, an outstandingly high efficiency of 7.68% was achieved from the TiO_2 films with novel structure, which was synthesized using 0.9 ml tetrabutyl titanate followed by 12 h of etching and 48 h $TiCl_4$ post-treatment.

Acknowledgements

This work is supported in part by the National Natural Science Foundation of China (No. 51372075, 51502084), Research Fund for the Doctoral Program of Higher Education of China (RFDP, No.20124208110006).

References

1. B. O' Regan, M. Grätzel, *Nature.,* 1991, **35,** 737-740.
2. M. Grätzel, *Acc. Chem. Res.,* 2009, **42,** 1788-1798.
3. C. P. Lee, R.Y. Lin, L. Y. Lin, C. T. Li, T. C. Chu, S. S. Sun, J. T. Lin, K. C. Ho, RSC Adv., 2015, **5,** 23810-23825.
4. J. J. Lin, Y. U. Heo, A. Nattestad, M. Shahabuddin, Y. Yamauchi, J. H. Kin, *Phys. Chem. Chem. Phys.,* 2015, **17,** 7208-7213.
5. J. J. Lin, A. Nattestad, H. Yu, Y. Bai, L. Z. Wang, S. X. Dou, J. H. Kim, *J. Mater. Chem. A.,* 2014, **2,** 8902-8909.
6. X. Yu, H. Wang, Y. Liu, X. Zhou, B. J. Li, L. Xin, Y. Zhou, H. Shen, *J. Mater. Chem. A.,* 2013, **1,** 2110-2117.
7. S. M. Wang, W. W. Dong, R. H. Tao, Z. H. Deng, J. Z. Shao, L. H. Hu, J. Zhu, X. D. Fang, *J . Power Sources*., 2013, **235,** 193-201.
8. Z. Q. Sun, J. H. Kim, Y. Zhao, D. Attard, S. X. Dou, *Chem. Commun.,* 2013, **49,** 966-968.
9. B. Liu, E. S. Aydil, *J. Am. Chem. Soc.,* 2009, **131,** 3985-3990.
10. J. T. Jiu, S. J. Isoda, F. M. Wang, M. Adachi, *J. Phys. Chem. B.,* 2006, **110,** 2087-2092.
11. P. L. Kuo, T. S. Jan, C. H. Liao, C. C. Chen, K. M. Lee, *J. Power Sources.,* 2013, **235,** 297-302.
12. S. H. Kang, S. H. Choi, M. S. Kang, J. Y. Kim, H. S. Kim, T. Hyeon, Y. E. Sung, *Adv. Mater.,* 2008, **20,** 54-58.
13. M. Zhu, L. Chen, H. B. Gong, M. Zi, B. Q. Cao, *Ceram. Int.,* 2014, **40,** 2337-2342.
14. H. Yu, J. Pan, Y. Bai, X. Zong, X. Y. Li, L. Z. Wang, *Chem. Eur. J*., 2013, **19,** 13569-13574.

15. S. S. Mali, H. Kim, C. S. Shim, W. R. Bae, N. L. Tarwal, S. B. Sadale, P. S. Patil, J. H. Kim, C. K. Hong, *CrystEngComm.,* 2013, **15,** 5660-5667.

16. Z. Q. Sun, J. H. Kim, Y. Zhao, F. Bijarbooneh, V. Malgras, Y. M. Lee, Y. M. Kang, S. X. Dou, *J. Am. Chem. Soc*., 2011, **133,** 19314-19317.

17. M. Q. Lv, D. J. Zheng, M. D. Ye, L. Sun, J. Xiao, W. X. Guo, C. J. Lin, *Nanoscale.,* 2012, **4,** 5872-5879.

18. M. Q. Lv, D. J. Zheng, M. D. Ye, J. Xiao, W. X. Guo, Y. K. Lai, L. Sun, C. J. Lin, J. Zuo, *Energy Environ. Sci.,* 2013, **6,** 1615-1622.

19. H. Wang, Y. S. Bai, H. Zhang, Z. H. Zhang, J. H. Li, L. Guo, *J. Phys. Chem. C*., 2010, **114,** 16451-16455.

20. H. Wang, B. Y. Wang, J. C. Yu, Y. X. Hu, C. Xia, J. Zhang, R. Liu, *Sci. Rep.,* 2015, **5,** 9305 (pp 9)

21. J. Zhang, S. Q. Li, H. Ding, Q. T. Li, B. Y. Wang, X. N. Wang, H. Wang, *J. Power Sources.,* 2014, **247,** 807-812.

22. J. Zhang, Q. T. Li, S. Q. Li, Y. Wang, C. Ye, P. Ruterana, H. Wang, *J. Power Sources.,* 2014, **268,** 941-949.

23. A. Kumar, A. R. Madaria, C. W. Zhou, *J. Phys. Chem. C.,* 2010, **114,** 7787–7792.

24. H. M. Cheng, J. M. Ma, Z. G. Zhao, L. M. Qi, *Chem. Mater*., 1995, **7,** 663–671.

25. L. Liu, J. S. Qian, B. Li, Y. M. Cui, X. F. Zhou, X. F. Guo, W. P. Ding, *Chem. Commun.,* 2010, **46,** 2402-2404.

26. N. G. Park, J. V. Lagemaat, A. J. Frank, *J. Phys. Chem. B*., 2000, **104,** 8989-8994 .

27. S. Powar, Q. Wu, M. Weidelener, A. Nattestad, Z. Hu, A. Mishra, P. Bäuerle, L. Spiccia, Y. B.

Cheng, U. Bach, *Energy Environ. Sci.,* 2012, **5,** 8896-8900.

28. H. M. Zhang, Y. H. Han, P. Liu, H. Yu, S. Q. Zhang, X. D. Yao, H. J. Zhao, *Chem. Commun.,* 2010, **46,** 8395-8397.
29. J. Kim, J. K. Koh, B. Kim, J. H. Kim. E. Y. Kim, *Angew. Chem.,* 2012, **124,** 6970-6975.
30. J. B. Na, J. H. Kim, C.Y. Park, E. Y. Kim, *RSC Adv.,* 2014, **4,** 44555-44562.
31. S. Hore, C. Vetter, R. Kern, H. Smit, A. Hinsch, *Sol. Energy Mater. Sol. Cells.,* 2006, **90,** 1176–1188.
32. H. J. Koo, Y. J. Kim, Y. H. Lee, W. I. Lee, K. Kim, N. G. Park, *Adv. Mater.,* 2008, **20,** 195-199.
33. Y. Tachibana, K. Hara, K. Sayama, H. Arakawa, *Che. Mater.,* 2002, **14,** 2527-2535.
34. L. Kavan, J. H. Yum, M. Grätzel, *ACS Nano.,* 2011, **5,** 165-172.
35. A. Hagfeldt, G Boschloo, L. C. Sun, L. Kloo, H. Pettersson, *Chem. Rev.,* 2010, **110,** 6595-6663.
36. J. Bisquert, A. Zaban, M. Greenshtein, I. Mora-Seró, *J. Am. Chem. Soc.,* 2004, **126,** 13550-13559.
37. A. Zaban, M. Greenshtein, J. Bisquert, *ChemPhysChem*., 2003, **4,** 859-864.
38. A. Sedghi, H. N. Miankushki, *Jpn J Appl.Phys.,* 2013, **52,** 075002 (pp1-5).
39. J. Liang, G. M. Zhang, W. T. Sun, *RSC Adv.,* 2014, **4,** 6746-6751.
40. D. B. Menzies, Q. Dai, L. Bourgeois, R. A. Caruso, Y. B. Cheng, G. P. Simon, L. Spiccia, *Nanotechnology,* 2007, **18,** 125608 (11p).

Figure captions

Fig. 1. SEM images of TiO_2 1D/3D nanorods followed by etching treatment in solution of 5 ml DI water and 11 ml concentrated hydrochloric acid at 150 ^oC for 8 h (a), 10 h (b), 12 h (c), 14 h(d), 16 h(e).

Fig. 2. The cross-sectional views of TiO_2 nanorod arrays in the bottom layer of TiO_2 1D/3D nanorods structure etched in solution of 5 ml DI water and 11ml concentrated hydrochloric acid at 150 ^oC for different duration 8 h (a), 10 h (b), 12 h (c), 14 h(d), 16 h(e).

Fig. 3. The X-ray diffraction pattern of un-etching (a) and 8 h etching TiO_2 films with network structure.

Fig. 4. (a) Diffuse reflectance spectra of TiO_2 films with network structure etched for different times before dye adsorption, the inset is the amplifying image for the scale of 600-900 nm (b) UV-vis absorbance spectra of dye-sensitized TiO_2 films for different times.

Fig. 5. (a)The photocurrent –voltage curve of the DSSCs based on TiO_2 films etched for different times measured under AM 1.5G solar irradiation of 100 mW/cm^2 (b) IPCE spectra of DSSCs based on TiO_2 films prepared at different etching time.

Fig. 6. (a) Open –circuit voltage decay measurement of the DSSCs based on TiO_2 network structure with different etching time. (b) The electron lifetime derived from equation (2) as a function of V_{oc}.

Fig. 7. The J-V characteristics of DSSCs based on TiO_2 network structure films which were synthesized using different titanium precursor and followed by etching treatment for 12 h.

Fig. 8. The top-view images of TiO_2 network structure immersed in the $TiCl_4$ solution for different

time. (a) 0 h (b)12 h (c)36 h (d) 48 h.

Fig. 9. The J-V curves of DSSCs based on TiO_2 network structure films immersed in the $TiCl_4$ solution for different times.

Table 1 photovoltaic parameters of DSSCs based on TiO_2 network structure with different etching duration.

sample	V_{oc} (V)	J_{sc} (mA/cm^2)	Fill Factor	Efficiency	Dye-loading ($nmol/cm^2$)
8 h	0.73	8.37	69.64	4.30	125.13
10 h	0.74	10.38	68.31	5.25	150.42
12 h	0.74	11.95	64.23	5.68	181.89
14 h	0.73	12.78	61.20	5.71	214.62
16 h	0.71	9.92	64.03	4.51	162.86

Table 2 detail photovoltaic properties of DSSCs based on TiO_2 network structure films synthesized using different amount of titanium precursor.

sample	V_{oc} (V)	J_{sc} (mA/cm^2)	Fill Factory	Efficiency
0.8 ml	0.72	8.62	57.84	3.59
0.9 ml	0.76	13.47	62.90	6.44
1.0 ml	0.74	11.95	64.23	5.68
1.2 ml	0.74	12.94	59.42	5.69

Table 3 photovoltaic parameters of DSSCs assembled by 12 h etching TiO_2 network structure films immersed in $TiCl_4$ solution for different times.

sample	V_{oc} (V)	J_{sc}(mA/cm^2)	Fill Factory	Efficiency
0h	0.76	13.47	62.90	6.44
12h	0.71	14.52	59.56	6.14
24h	0.71	16.96	58.30	7.02
48h	0.72	18.30	58.29	7.68

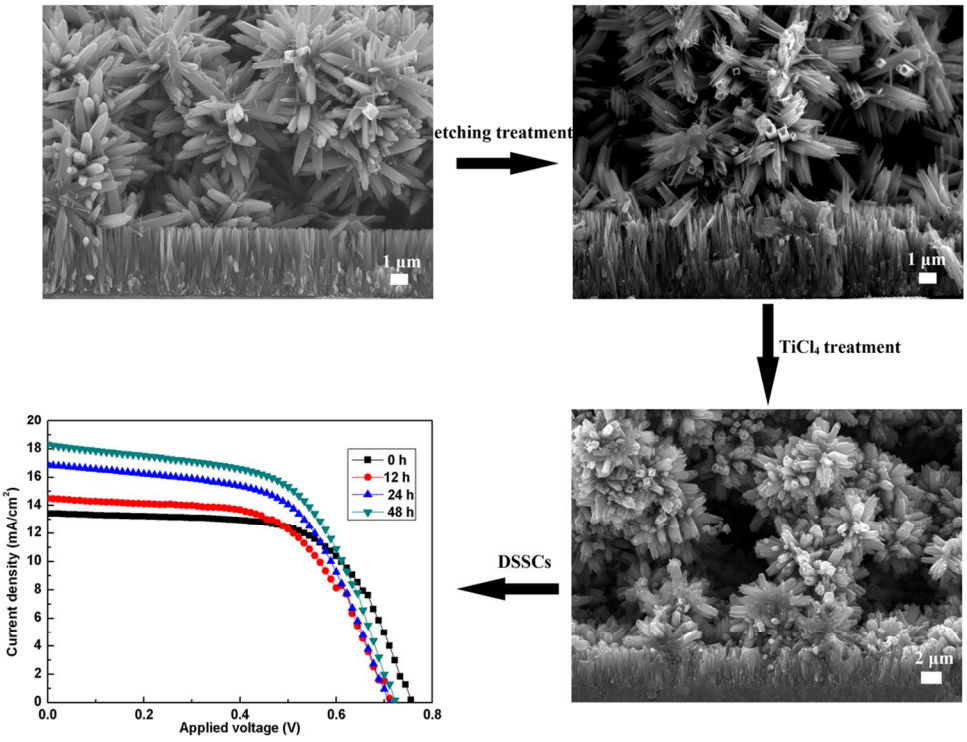

462x343mm (72 x 72 DPI)

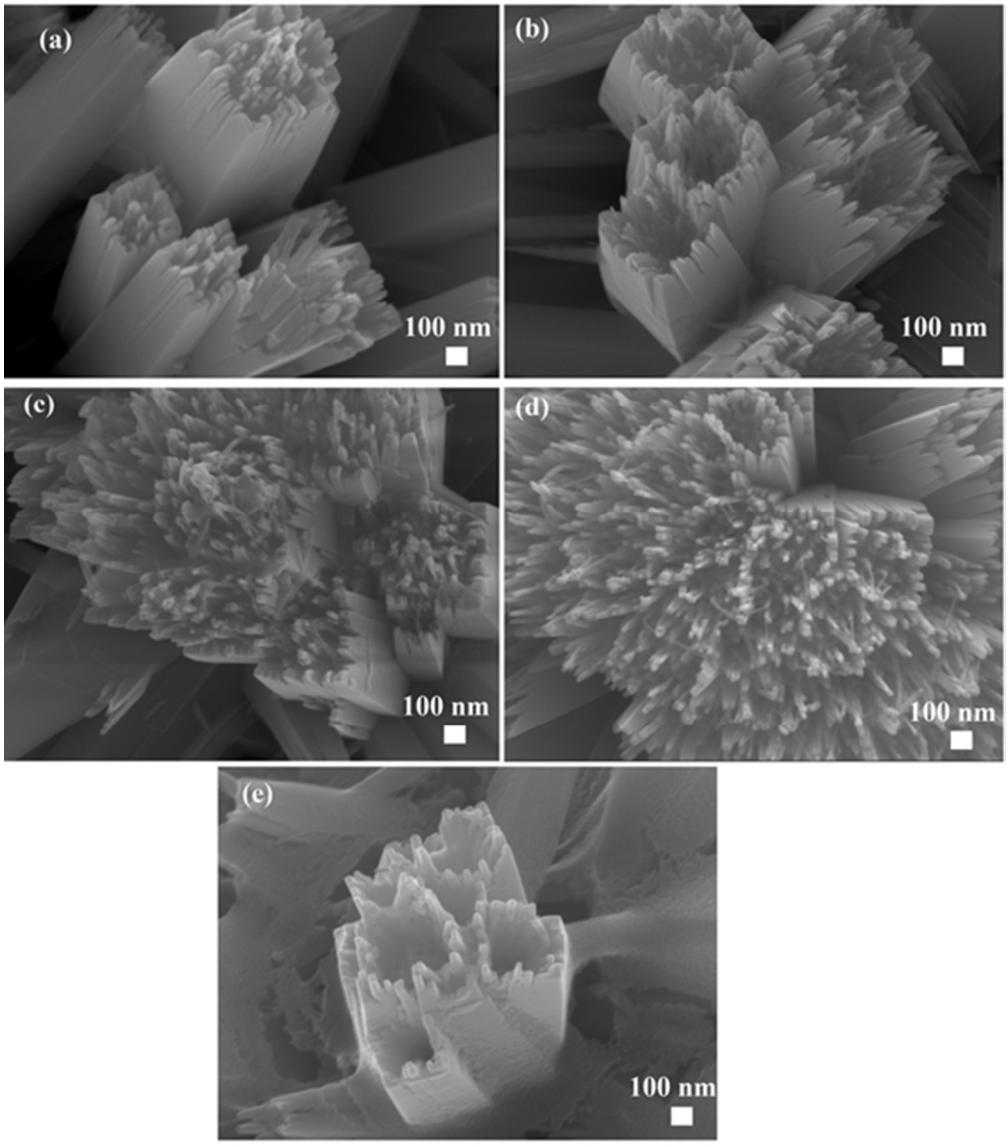

Figure 1
50x58mm (300 x 300 DPI)

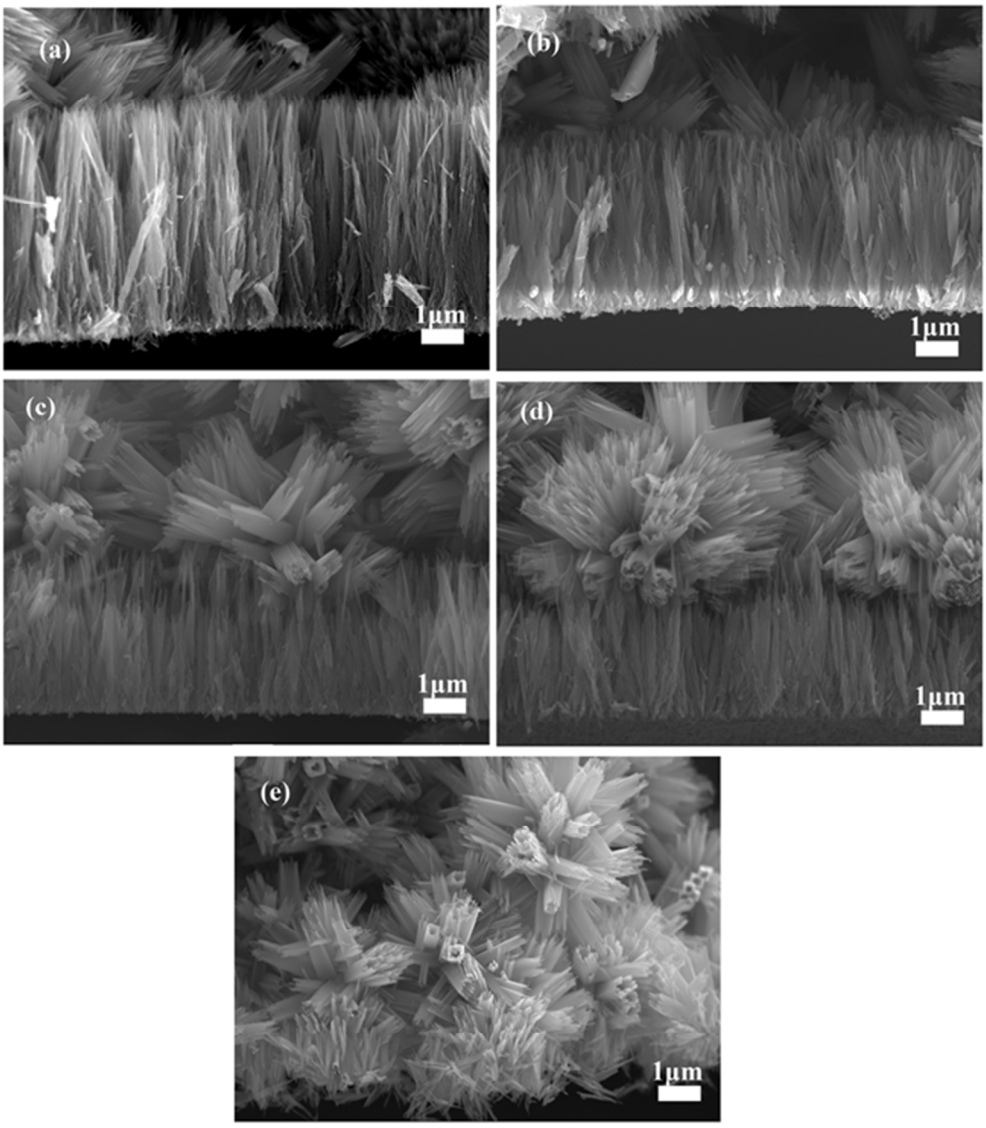

Figure 2
55x63mm (300 x 300 DPI)

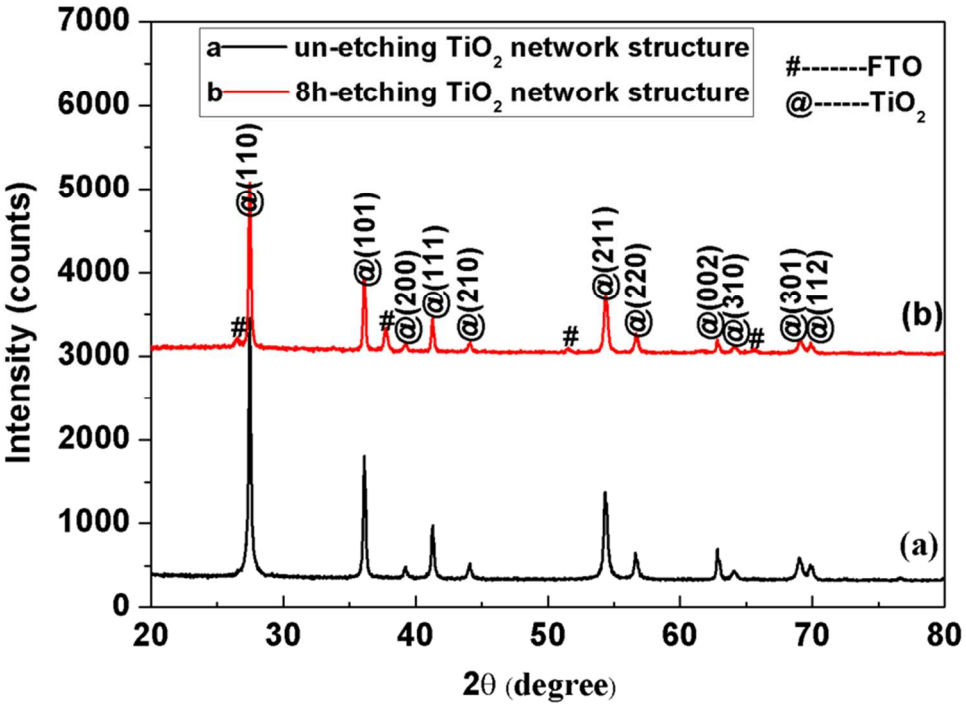

Figure 3
80x57mm (300 x 300 DPI)

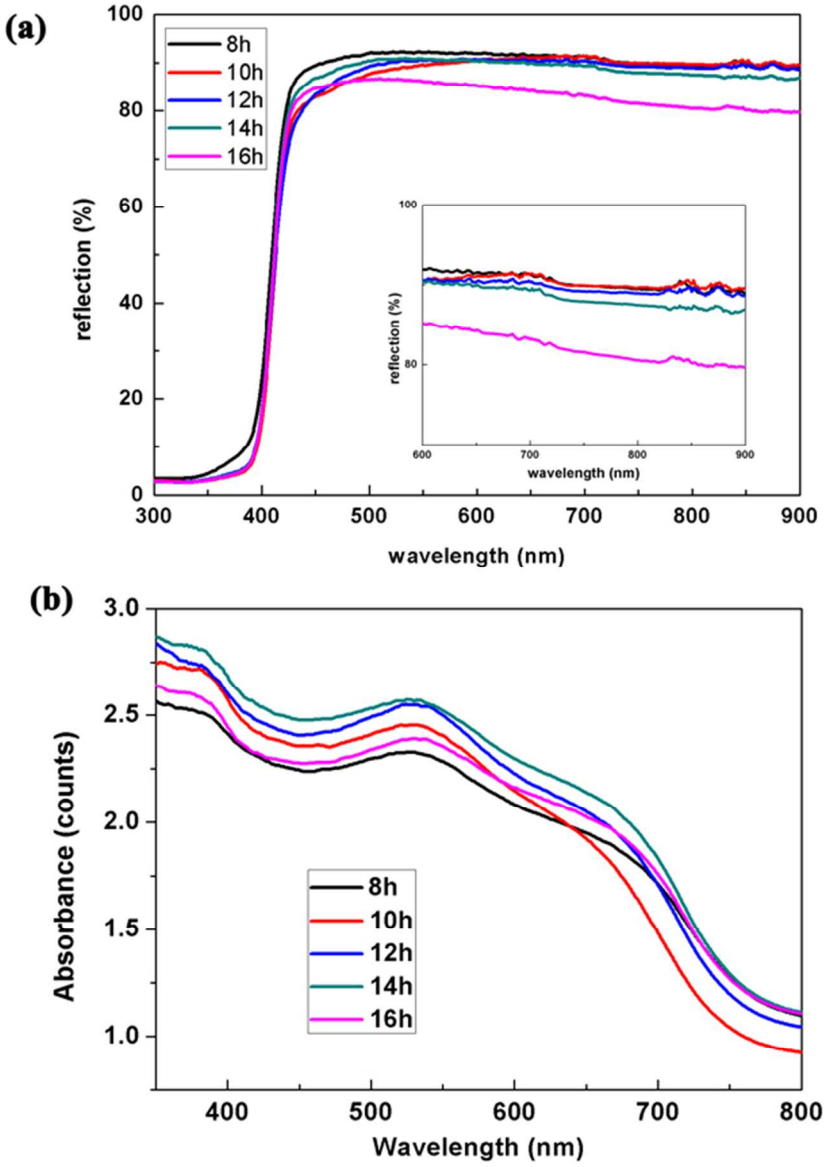

Figure 4
54x75mm (300 x 300 DPI)

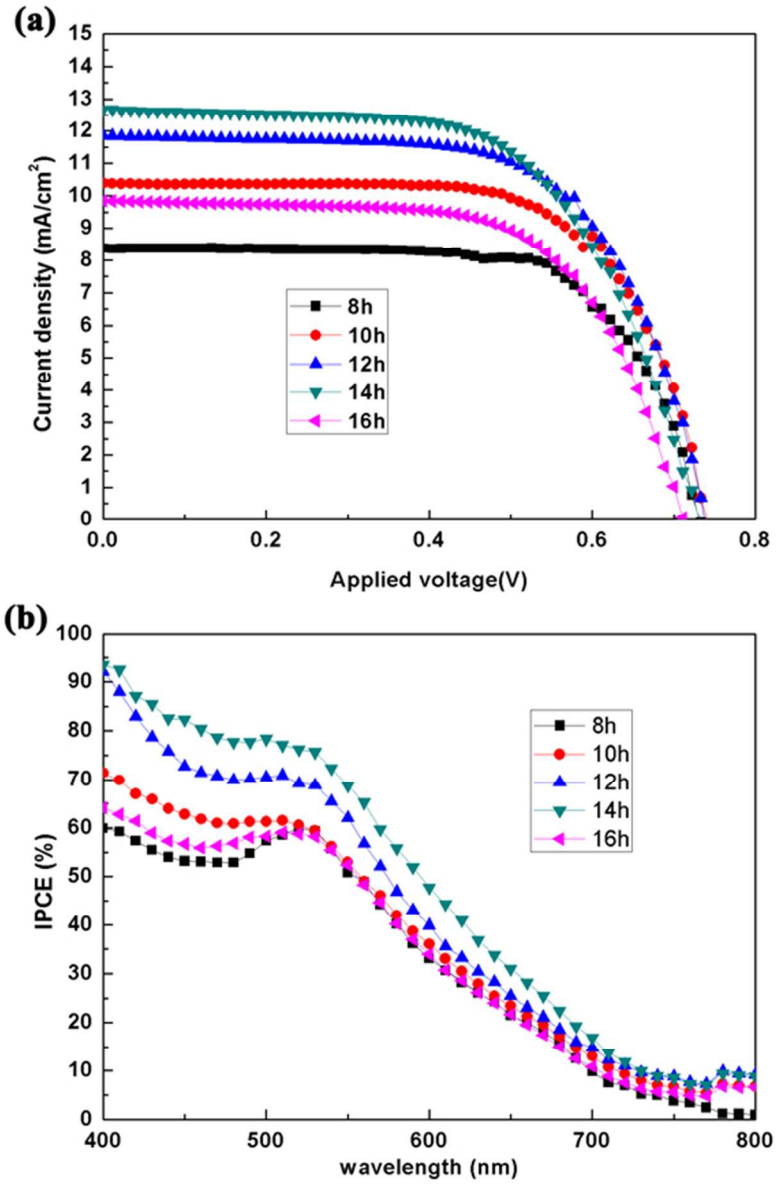

Figure 5
49x74mm (300 x 300 DPI)

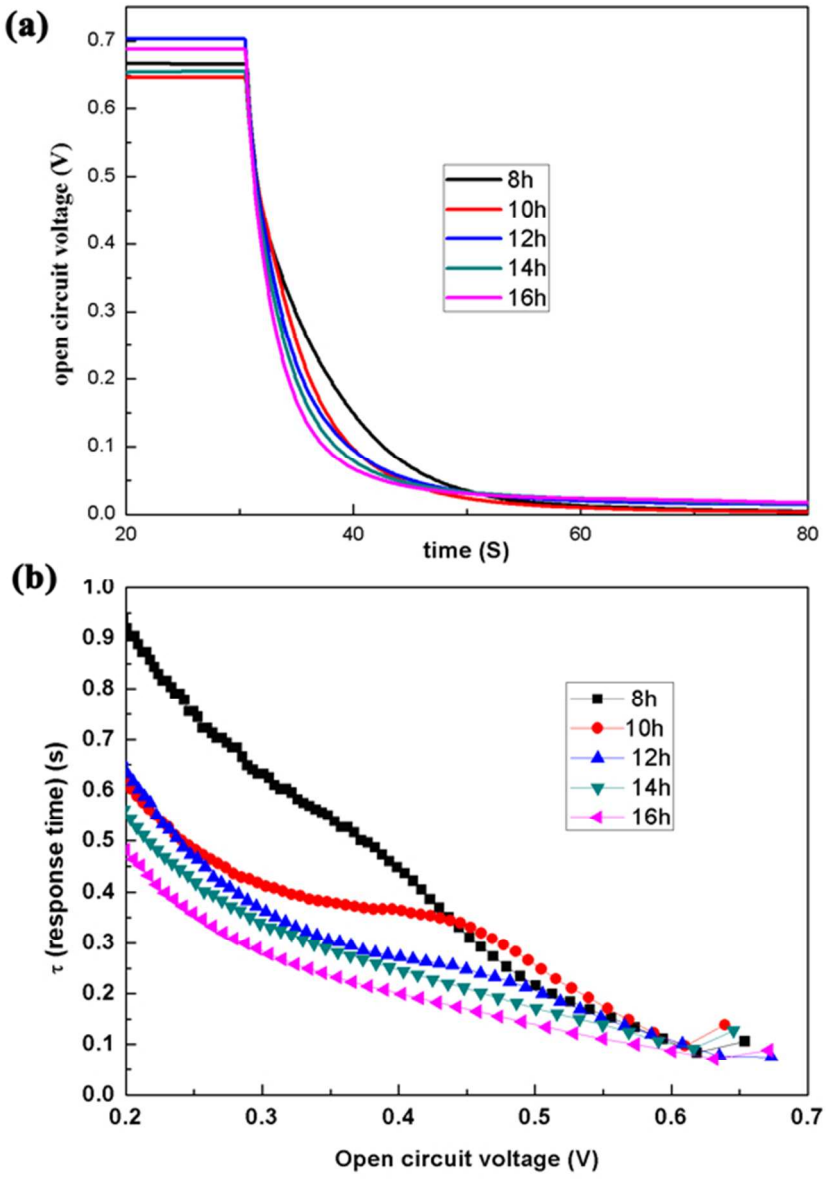

Figure 6
50x71mm (300 x 300 DPI)

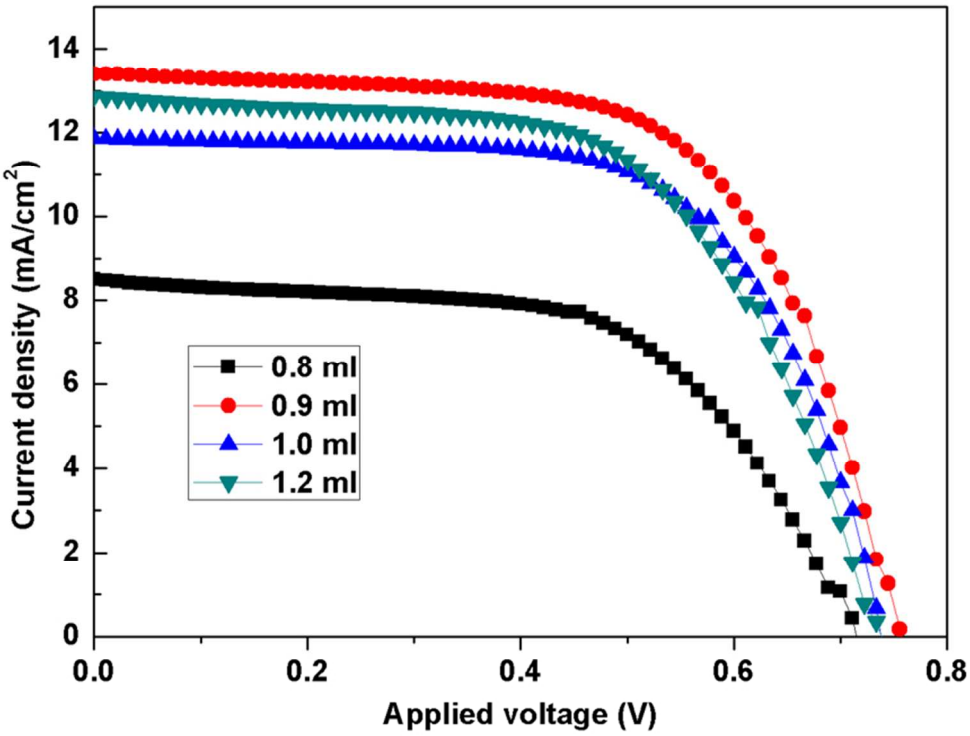

Figure 7
75x59mm (300 x 300 DPI)

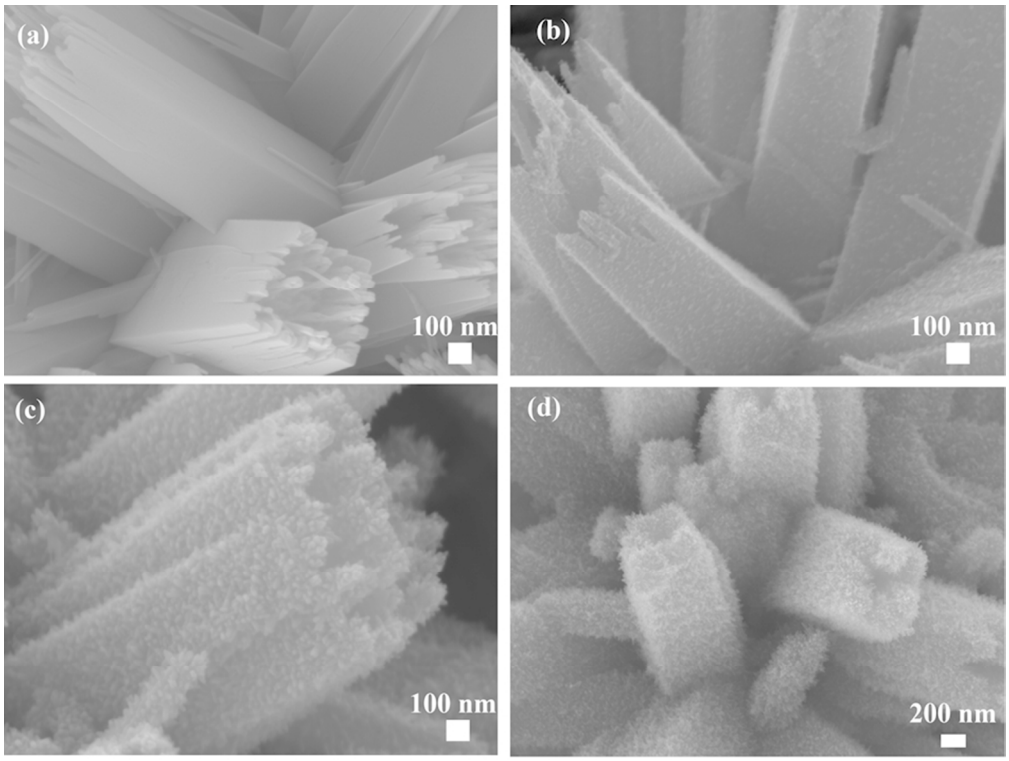

Figure 8
80x60mm (300 x 300 DPI)

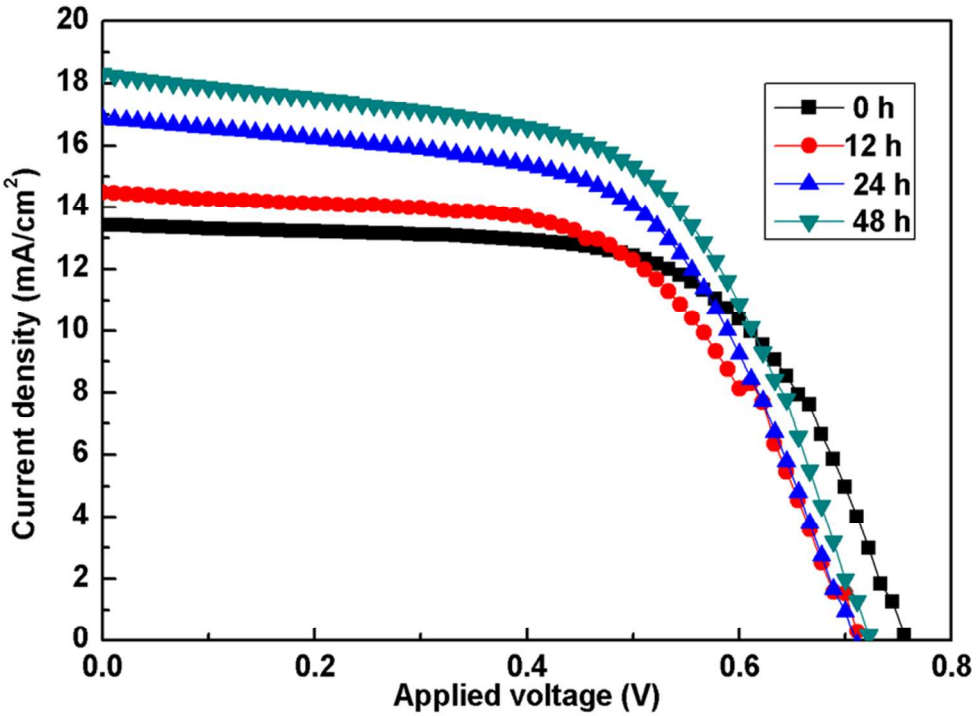

Figure 9
75x55mm (300 x 300 DPI)